UDK 621.396

DESCRIPTIVE EXPERIMENT DESIGN FRAMEWORK FOR HIGH RESOLUTION IMAGING WITH MULTIMODE ARRAY RADAR SYSTEMS

V. ESPADAS AND Yu. SHKVARKO

We address a descriptive experiment design (DED) regularization approach for enhanced resolution imaging of multiple targets via space-time processing of multimode array radar (MAR) data. The multiple frequency-polarization signal processing (SP) mode is employed to provide necessary DED redundancy that is next exploited to enhance the MAR imaging resolution performances in different operational environments including harsh scenarios with imperfect array calibration, partial sensor failure and/or uncertain noise statistics. The proposed DED framework provides robust extension of the Van-Zittert — Zernike approach based on the matched spatial filter bank SP for such realistic operational scenarios. The DED-based MAR employs the robust regularized matched spatial filter bank SP for image formation, in which the shape of the MAR resulting point spread function is optimized applying the new proposed DED-inspired quality metrics constructed to optimally balance the resolution-over-noise-suppression performances adapted to harsh multiple target sensing scenarios. Numerical simulations verify the effectiveness of the proposed DED-SP method for MAR imaging in harsh sensing environments.

Keywords: antenna ray, descriptive experiment design, multimode imaging radar, regularization.

INTRODUCTION

Sensor array signal processing (SP) for imaging radars has been the focus of tremendous theoretical advances and application developments in the last decades and many sophisticated techniques are now available (see, for example [1]–[6] and the references therein). In the imaging radar science, new trends relate to employment of multiple processing modes that provide the necessary data redundancy that can be next exploited to enhance the overall multimode array radar (MAR) imaging resolution performances. Crucial still unresolved MAR-SP issues relate to robust enhanced imaging in harsh operational scenarios characterized by possible imperfect array calibration, partial sensor failure and/or uncertain noise statistics.

In this study, we address a new descriptive experiment design regularization approach for enhanced resolution imaging of multiple targets via space-time processing of MAR system data. The multiple frequency-polarization SP mode is employed to provide necessary DED redundancy in the considered harsh operational scenarios. At the hardware (HW) design level, the crucial problem relates to optimization of the sensor array configuration aimed at approaching the desired resulting point spread function (PSF) performances, e.g., the lowest possible side-lobes level balanced over the minimum effective width of the main PSF beam. At the software (SW) design level, the further problem is to develop the robustified matched spatial filter (MSF) bank image formation techniques aimed at approaching the overall high-resolution MAR imaging performances. To approach these HW-SW co-design goals, we propose the descriptive experiment design (DED) framework constructed via robust extension of the Van-Zittert-Zernike approach based on the MSF bank SP. The shape of the MAR system PSF is optimized applying the new proposed DED-inspired quality metrics constructed to satisfy the balanced resolution-over-noise suppression requirements adapted to high resolution multiple target sensing scenarios. We analyze the achievable PSFs for a variety of admissible MAR-SP mode specifications [4], [5], that is, different inter-sensor distance and various carrier frequencies and polarization modes. This study establishes a DED framework for MAR imaging HW system design in terms of new resolution metric that controls the minimization of the resolution cells balanced over the suppression of the PSF grating sidelobes. Next, the DED-based SW level SP performs the robust regularized image formation with the optimized PSF shape. Last, the numerical simulations verify the effectiveness of the proposed DED-SP method for MAR imaging in harsh sensing environments.

I. GEOSTAR-CONFIGURED MAR SYSTEM SPECIFICATIONS

The so-called GeoSTAR (Geo synthesized thinned array radiometer) imaging sensor system has been originally addressed in [1] as a concept to provide high resolution imaging of distributed RS scenes with passive microwave and mm waveband radiometers. Nevertheless, the celebrated GeoSTAR array configuration is also well adapted for active MAR systems as it was demonstrated in [6], [11].The particular imaging MAR system under consideration in this study is a multimode array sensor system of [6], [11]. Such MAR operates at two separate yet concurrent frequencies of 24.5 GHz and 35 GHz with dual polarization (V – vertical and H – horizontal). At one instant, radio frequency (RF) pulses of a specified pulse width (PW) are transmitted concurrently at 24.5 and 35 GHz in either V polarization or H polarization. These pulses are "calibrated" to maintain coherency so that their amplitudes and phases are constant for different pulses. The transmitting antenna is switched between vertical (V) and horizontal (H) polarizations, i.e., V and H transmitted pulses are delayed by a certain time. For each frequency (24.5 GHz or 35 GHz), transmitted V polarized and H polarized RF

pulses are separated by a half of the fixed pulse repetition time (PRT/2) as illustrated in Fig.1.

The antenna array is composed of 24 elements as in [1], [6]; each sensor element receives signals at V and H polarizations. The received signals are spread over time duration of N PWs, where N is the number of range resolution cells used to process the received signals for each transmitted pulse. In every PRT corresponding to one frequency band (24 GHz or 36 GHz), one time delay vector $\mathbf{T_d}$ and 4 measurement data vectors, $\mathbf{U_{VV}}$, $\mathbf{U_{VH}}$, $\mathbf{U_{HV}}$, $\mathbf{U_{HH}}$, are provided for further processing. That is, for each polarization modes (VV, VH, HV or HH) there is no time delay between receiving antenna elements since they are spaced close to each other, so $\mathbf{T_d}$ has only one value for all 24 elements for each received signal. Each data vector $\mathbf{U_{VV}}$ ... $\mathbf{U_{HH}}$ contains the relevant in phase (I) and quadrature (Q) components that compose 24 rows data ($i = 1 \rightarrow 24$) collected for $2N$ measurement time instants ($n = 1 \rightarrow N$). The transmit-receive format is explained in Fig. 2. The operation range of the MAR system is in the interval from 1m to 50m, with a range resolution cell of 0.3m, so at the SP level the observer controls 165 overall range processing gates.

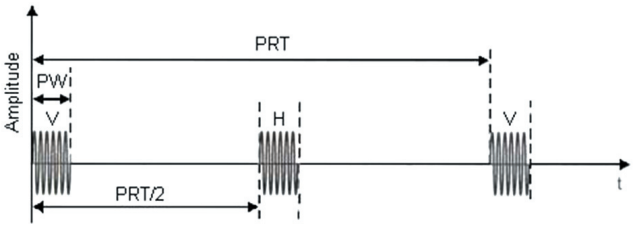

Fig. 1. Transmit RF pulse format

The crucial SP issue relates to the formation of the empirical estimate $\mathbf{Y}_r = \underset{i}{aver}\{\mathrm{U}_r(i)\mathrm{U}_r^+(i)\}$ of the sensor data true correlation matrix $\mathbf{R}_r = <\mathrm{U}_r\mathrm{U}_r^+>$ for each range gate $r = 1, ..., R_r = 165$. The independent realizations $\{\mathrm{U}_r(j);\ j = 1,...,J\}$ in the averaging procedure for formation of $\mathbf{Y}_r$ are to be recorded over J transmitted pulses for each range gate $r = 1, ..., R_r = 165$. To guarantee the full-rank sensor data covariance matrices $\{\mathbf{Y}_r, r = 1,..., R\}$ the minimal number of independent recordings J should be not less than the number of sensors ($M = 24$), thus $J > 24$ independent realizations are to be recorded for each range gate $r = 1, ..., R_r = 165$. In the opposite case, $J < 24$, the data covariance matrices are rank-deficient. This means that for $J < 24$ the robust MSF-based beamforming for sensor focusing inevitably faces the problem of huge artifacts (so called ghosts on the speckle corrupted scene images [5], [8]). At the target detection SP stage, such artifacts inevitably increase the false alarm rate [8]. That is why, in all SP developments in this study, the redundancy guaranteed SP mode $J > 24$ is considered.

To compare different HW designs, in this study we analyze three feasible sensor array configurations. Fig. 3(a) shows the conventional X-shaped equally-spaced antenna array layout for the inter-element spacing $d_{A(1)} = 0.5\,\lambda_o$, where λ_o specifies the employed wavelength, in this case $f_o = 24$ GHz. The corresponding so-called *uv* spatial samples in the *visibility* domain are presented in Fig. 3(b). In Fig. 4(a), a circular-shaped (O-shaped) antenna array layout with the same parameters is depicted. The related *uv* spatial visibility samples are shown in Fig. 4(b). The GeoSTAR Y-shaped antenna array is presented in Fig. 5(a) with the corresponding *uv* samples in Fig 5(b), respectively. In all cases, u and v samples specify the normalized (so-called *visibility* domain) coordinate representation format, i.e., $u = x/\lambda_o$, and $v = y/\lambda_o$.

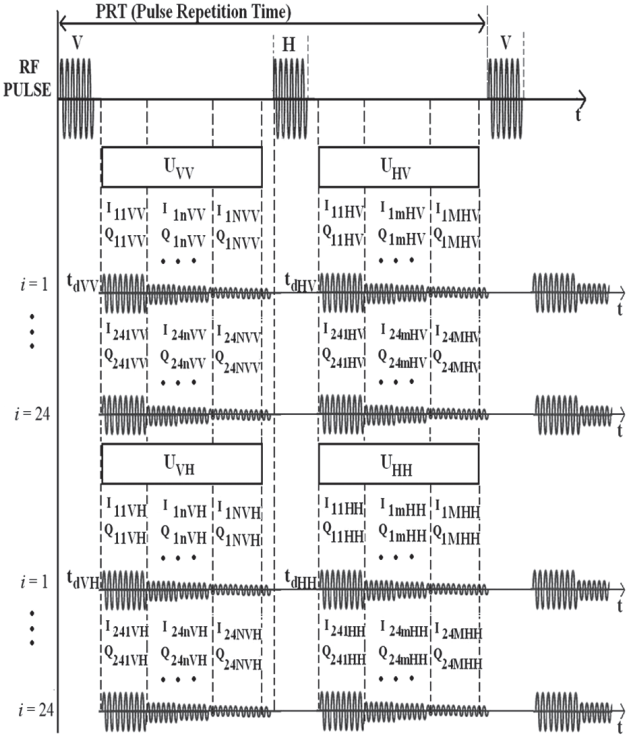

Fig. 2. Transmit-receive signal format

II. MSF IMAGE FORMATION TECHNIQUE

The proposed MSF-based image formation algorithm comes directly from the celebrated Van-Zittert-Zernike theorem from radio astronomy [6], [8] according to which, the noise-free data visibility function $R(u,v)$ (constructed directly from the noise free data true covariance function $R(x,y)$ at each range gate via its scaling to the visibility domain [6]) and the related spatial spectrum pattern (SSP) or angular brightness distribution $b(\theta_x,\theta_y)$ over the 2-D angular observation space $(\theta_x,\theta_y) \in \Theta$ are related through the 2-D spatial inverse Fourier transform:

$$R(u,v) = c\Im_\theta^{-1}\left\{b(\theta_x,\theta_y)\right\} = c\int_\Theta b(\theta_x,\theta_y)\exp\left[+i2\pi(u\theta_x + v\theta_y)\right]d\theta_x\,d\theta_y, \quad (1)$$

where c is the normalizing constant [6] (not critical for image formation and analysis) and the visibility function arguments (u, v) represent the x–y projections of the normalized sensor *baseline* vectors (normalized to the wavelength λ_o) in the visibility domain $(u, v) \in P/\lambda_o$ [6], [8].

The robust MSF-based method [4], [5] for RS image formation implies, first, formation of the

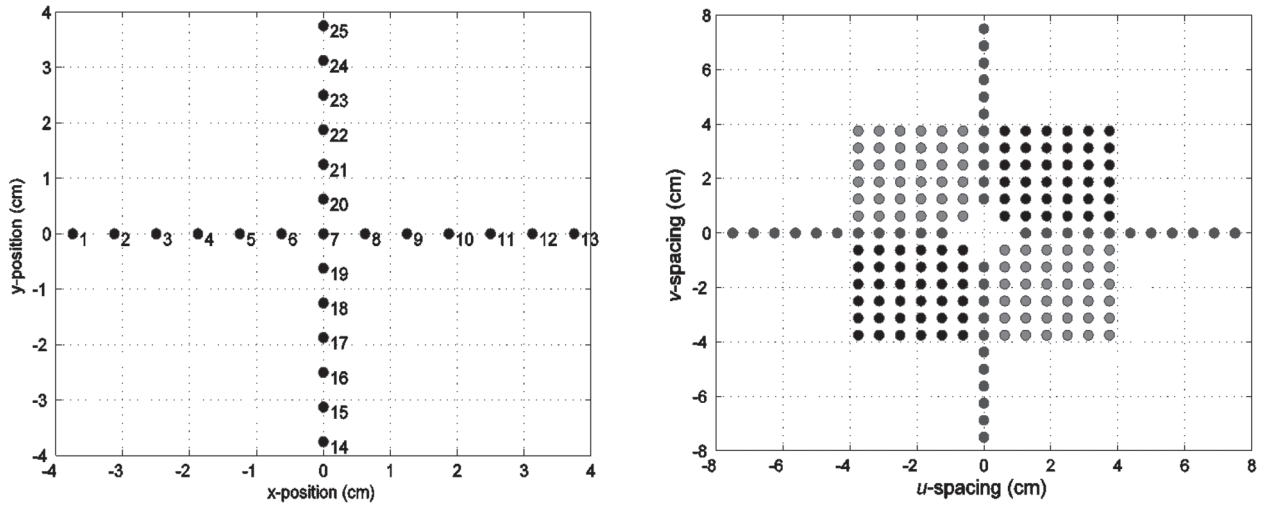

(a) (b)

Fig. 3. (a) Antenna array layout with sensor numbering for X-shaped configuration;
(b) corresponding *uv* samples for inter-element spacing $d_{A(1)} = 0.5\lambda_o$; carrier frequency $f_o = 24$GHz

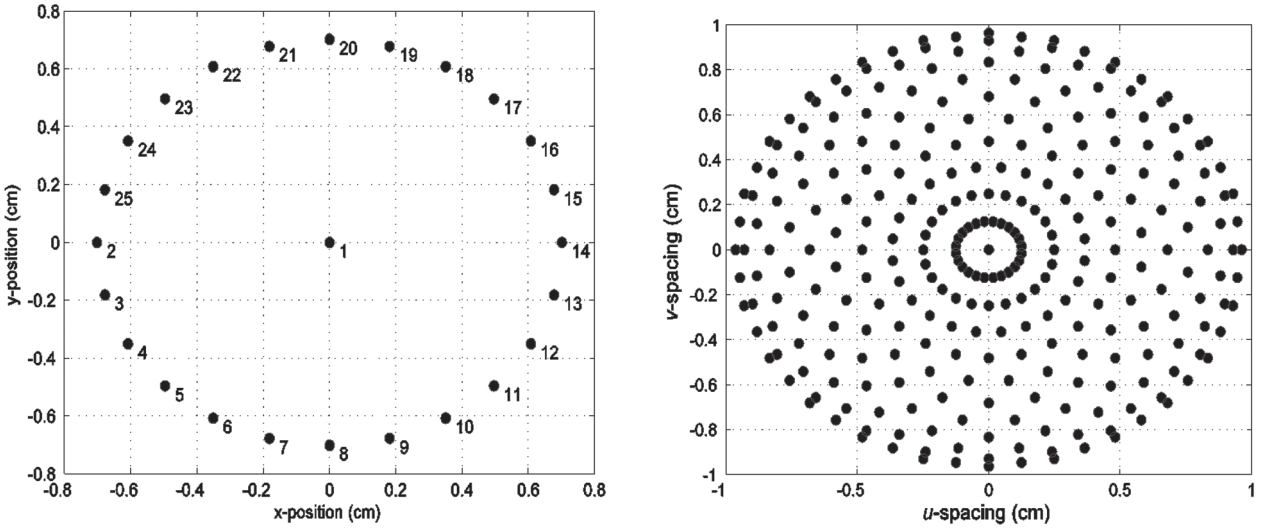

(a) (b)

Fig. 4. (a) Antenna array layout with sensor numbering for O-shaped configuration;
(b) corresponding *uv* samples for inter-element spacing $d_{A(1)} = 0.5\lambda_o$; carrier frequency $f_o = 24$GHz

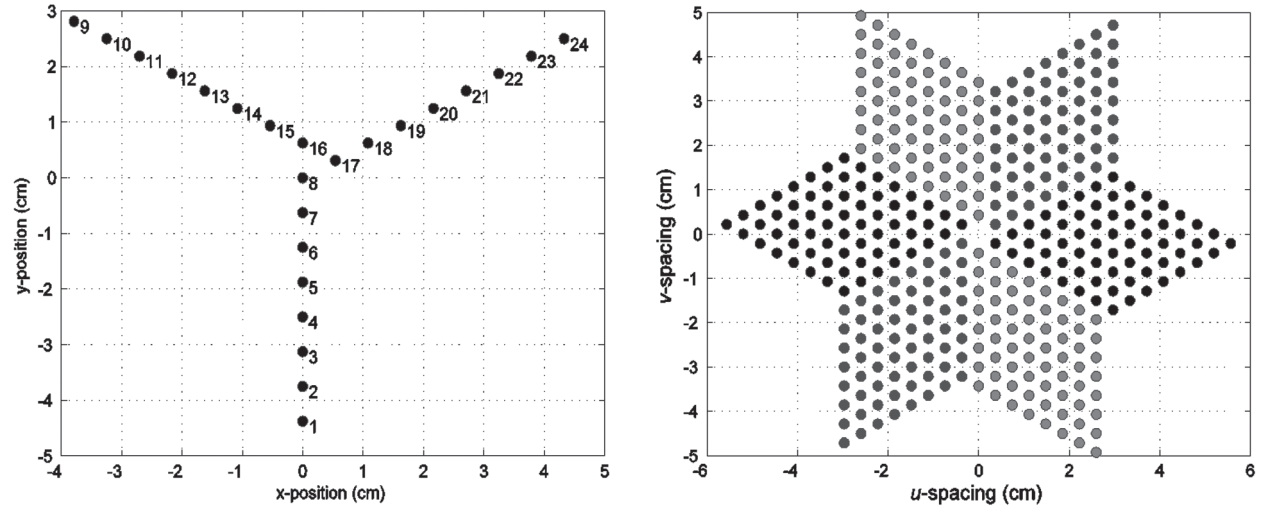

(a) (b)

Fig. 5. (a) Antenna array layout with sensor numbering for Y-shaped GeoSTAR configuration;
(b) corresponding *uv* samples for inter-element spacing $d_{A(1)} = 0.5\lambda_o$; carrier frequency $f_o = 24$GHz

observed noised visibility function $\hat{R}(u,v)$ via scaling the estimated correlation matrix $\mathbf{Y}_r$ to the visibility domain (over a range of normalized visibility spacings $(u,v)\in P/\lambda_o$) followed, second, by the 2-D Fourier transform that yields the MSF image of the scene

$$\hat{b}(\theta_x,\theta_y)=\Im_{u,v}\left\{\Pi_{A(u,v)}\hat{R}(u,v\,|\,r)\right\}= \int_R \Pi_{A(u,v)}\hat{R}(u,v\,|\,r)\exp\left[-i2\pi(u\theta_x+v\theta_y)\right]d\theta_x\,d\theta_y \quad (2)$$

at a particular rth range gate from the range observation domain $R\ni r$ [2]. Here, the projector $\Pi_{A\{u,v\}}$ specifies the particular employed sensor array configuration resulting in different resolution performances attainable with the MSF-based imaging technique (2). In the pursued here nonparametric problem treatment, such resolution quality is assessed by the shape of the resulting system PSF associated with the image (2) of a single point-type target located at the scene origin at the corresponding range gate $r\in R$. In particular, the desired system PSF is associated with the shape that provides the lowest possible side lobes (and grating lobes) level balanced over the minimum achievable effective width of the PSF main beam [7], [9], [10].

Based on (2), let us next analyze the PSFs of the MAR imaging systems attainable with the employment of the conventional X-shaped, O-shaped array and the celebrated GeoSTAR-configured Y-shaped array. In Figures 6 thru 8, we present the PSFs related to the MSF-based single target (TAG) imaging procedure (2) employing the cross-shaped (X-shaped) [6], circular-shaped (O-shaped) [10] and the GeoSTAR-configured Y-shaped sensor array [1], [11] geometries in the terms of the attainable angular PSF of the corresponding MAR imaging systems. The PSF cross-sections in the x-y imaging scene provide explicit information on the spatial resolution cells achievable with such differently configured imaging sensor arrays that employ the conventional 2-D MSF method (2) for RS image formation. In Fig. 6, we present the PSF for the conventional X-configured imaging array with the inter-element spacing $d_{A(6)} = 2\lambda_o$, i.e., equal to the double of the carrier wavelength (for the carrier frequency f_0 = 24 GHz), while in Fig. 7 the PSF for the O-configured array with the same parameters is depicted. Next, in Fig. 8, the PSF for the Y-shaped (GeoSTAR-configured) imaging array with the same parameters as the previous two PSFs is presented. Note that the most important characteristics of these PSFs are the width of the main beam and the maximum level of the secondary lobes (including the suppressed grating lobes). The simulations were next performed using the elaborated virtual remote sensing laboratory (VRSL) software [6], which are indicative of the usefulness of the HW-level DED-optimization of the multi-target scene imaging tasks via configuring the multi-mode sensor arrays employed in the particular RS array radar imaging systems. Fig. 9 shows the results of simulations of the DED-optimized multiple target scene imaging performed applying the 2-D MSF technique (2). The multiple target scene is composed of 5 targets (5 TAGs) in the particular simulated range gate (r = 30m) and the corresponding scene images are depicted in the x-y plane for the employed X, O and the Y (GeoSTAR) imaging sensor array configurations. The particular MAR operational sensing parameters employed in the reported simulations are specified in the figure captions.

III. OPERATIONAL UNCERTAINTIES

In this section, we treat two types of operational scenario uncertainties, in particular, possible sensor displacements and data failure due to some disabled sensors. We present a brief description of these operational uncertainties as well as an analysis of the image degradations that may suffer the MSF-based MAR-SP procedure (2) assuming such harsh scenarios.

A. Displaced Sensors

In Fig. 5(a) the MAR antenna layout was depicted; at this point it is important to fix the locations and the spacing between the elements of the antenna array. These positional characteristics are vital to compose the visibility function as shown in Fig. 5(b).

The sensor displacements (shifts) may occur due to damage or manufacturing errors. A sensor shift implies that the sensor's centroid is not in the correct coordinate position specified by the HW design. Assuming that a sensor is displaced at a quantity between the interval $[-\lambda_0/4, \lambda_0/4]$ for both coordinates x and y, we define now a vector $\tilde{p}_m$ wich characterizes the position of such displaced sensor

$$\tilde{p}_m=(x_m,y_m)+(x_{\Delta m},y_{\Delta m}) \quad (3)$$

where (x_m, y_m) are the correct (HW calibrated) coordinates of the sensor and $(x_{\Delta m},y_{\Delta m})$ represents the coordinate shifts. When adding these new parameters to the original procedure (2), we obtain the following MSF imaging result

$$\hat{b}(\theta_x,\theta_y\,|\,r)= \int_R \Pi_{A(u,v)}\hat{R}(u,v\,|\,r)\exp\left[-i2\pi(u\theta_x+v\theta_y)\right]\exp\{i2\pi[\tilde{\rho}_m,\theta]\}du\,dv \quad (4)$$

which contains the phase shift error term $\exp\{i2\pi[\tilde{\rho}_m,\theta]\}$ dependent on the inner product $[\tilde{\rho}_m,\theta]$. When a sensor is not shifted, this phase factor is equal to 1, that results in the original undistorted imaging procedure (2).

B. Disabled Sensors

As we mentioned in the previous section, the certain operational scenario presumes active functioning of all array sensors, i.e., all sensors must provide the measurement signal data signals needed to form the sensor data cross-correlation matrices ($\mathbf{Y}_r$ at all R range gates) and the related visibility functions. If one or more sensors in the array are disabled, the loss of data would cause a malformation of the matrix $\mathbf{Y}_r$, hence, inevitably distorted imaging via the MSF procedure (2). To relax the influence of such distortions, we perform the DED-based robustification of the

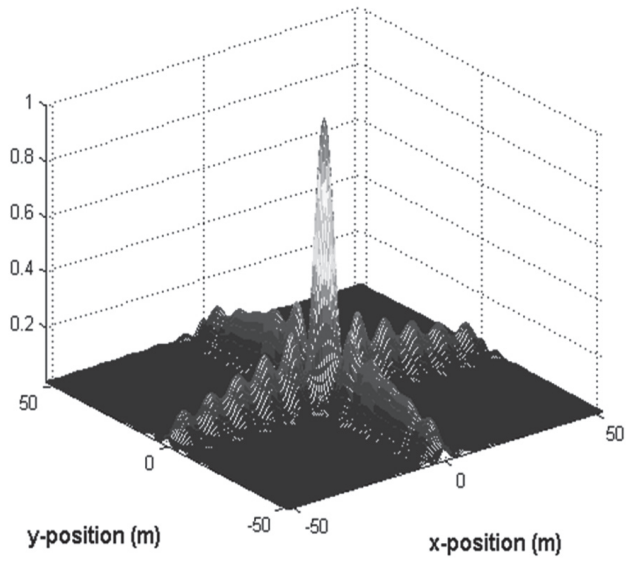

Fig. 6. Point Spread function (PSF) for 24 element X-shaped configured imaging array with $2\lambda_o$ inter-element spacing for 30m range gate

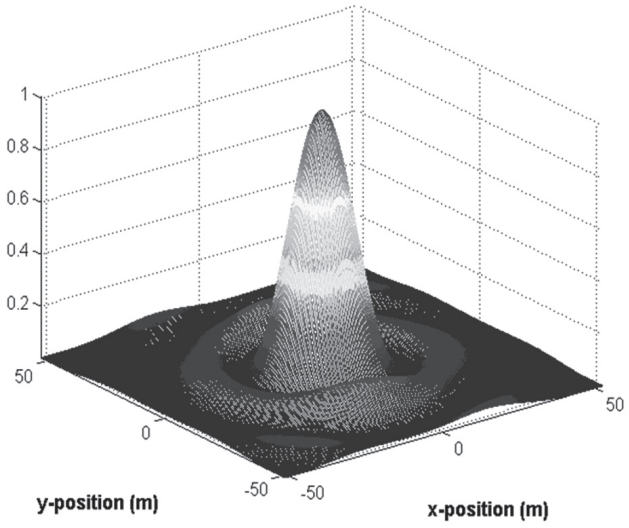

Fig. 7. Point Spread function (PSF) for 24 element O-shaped configured imaging array with $2\lambda_o$ inter-element spacing for 30m range gate

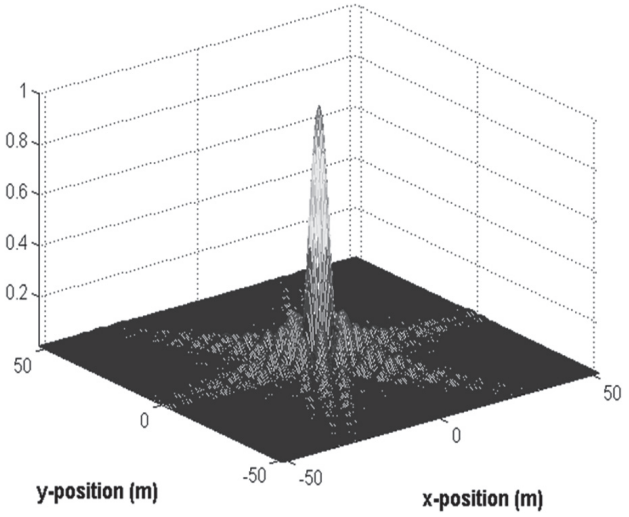

Fig. 8. Point Spread function (PSF) for 24 element Y-shaped configured imaging array with $2\lambda_o$ inter-element spacing for 30m range gate

covariance matrix $\mathbf{Y}_r$ at all R range gates following the sparse diagonal structuring regularization [11]. Fig. 10 shows the DED sparsified [11] structure of matrix $\mathbf{Y}_r$ for a fixed ($r = 30$m) range gate.

This sparse signal correlation matrix is composed of six active data blocks of 8-by-8 matrices and three zero-structured diagonal blocks $\underline{\mathbf{0}}_{(8x8)}$ composed of zeros. Three upper data blocks (sector S1, sector S2 and sector S3) relate to the sectors that correspond to the GeoSTAR unique baselines. The three lower data blocks (sector S4, sector S5 and sector S6) correspond to the symmetrical (virtual) GeoSTAR baselines composed by correlations between sensors of different arms of the antenna array. Last, three zero blocks $\underline{\mathbf{0}}_{(8x8)}$ located along the principal diagonal of the DED-sparse matrix $\mathbf{Y}_r$ correspond to the baselines between arms A1-A1, A2-A2 and A3-A3 that are *not* incorporated in the DED regularized processing algorithm (2) [11]. The complete set of measurements that compose matrix $\mathbf{Y}_r$ are applied in (2), but when one sensor or more are disabled, the DED-sparse matrix $\mathbf{Y}_r$ with the structure of Fig. 10 cannot be composed yielding possible undesirable processing results. In an illustrative interpretation, if sensor 1 of arm 1 is disabled, the first row of the sub matrices S1 and S2 (see Fig. 10) will be completely lost, along with their corresponding symmetric virtual elements in sub matrices S5 and S5.

To tackle with such harsh operational scenario uncertainties we address two DED inspired proposals. The first one is to perform an interpolation between the rows and the columns next to the missing elements in the matrix $\mathbf{Y}_r$ in a sparse form as shown in Fig. 10. When the sensor $m' = k$ presents a signal failure, the following interpolation is to be performed

$$\tilde{\mathrm{Y}}_r(k,m') = \frac{\mathrm{Y}_r(k+1,m') + \mathrm{Y}_r(k-1,m')}{2} \qquad (5)$$

$$\text{for } m' = 1, \ldots, M;\ M = 24.$$

This new interpolated matrix $\tilde{\mathrm{Y}}_r(k,m')$ is constructed for replacing the distorted matrix $\mathbf{Y}_r$, and next, the DED-MSF image formation procedure (2) is performed.

The second DED inspired approach is based on the 4-nearest neighbor interpolation (4-NNI) technique [11]. This technique is applied to fill in the lost data directly in the visibility function domain related to the distorted matrix $\mathbf{Y}_r$ (see Fig. 5(b)). In Fig. 11, we explain the 4-NNI procedure in a graphical form in the visibility domain. The lost data row is displayed as empty dots in the visibility function, and the applied 4-NNI technique consists in averaging four nearest sensors data measurements to interpolate the concerned empty data slot (u-v sample). This is done performing the following

$$\tilde{\mathrm{Y}}_r(k,m') = \frac{1}{4}\big(\mathrm{Y}_r(k-1,m'+1) + \mathrm{Y}_r(k-1,m') + \\ + \mathrm{Y}_r(k+1,m') + \mathrm{Y}_r(k+1,m'-1)\big) \qquad (6)$$

$$\text{for } m' = 1, \ldots, M;\ M = 24.$$

Our next objective is to determine the maximal number of disabled sensors with which the DED

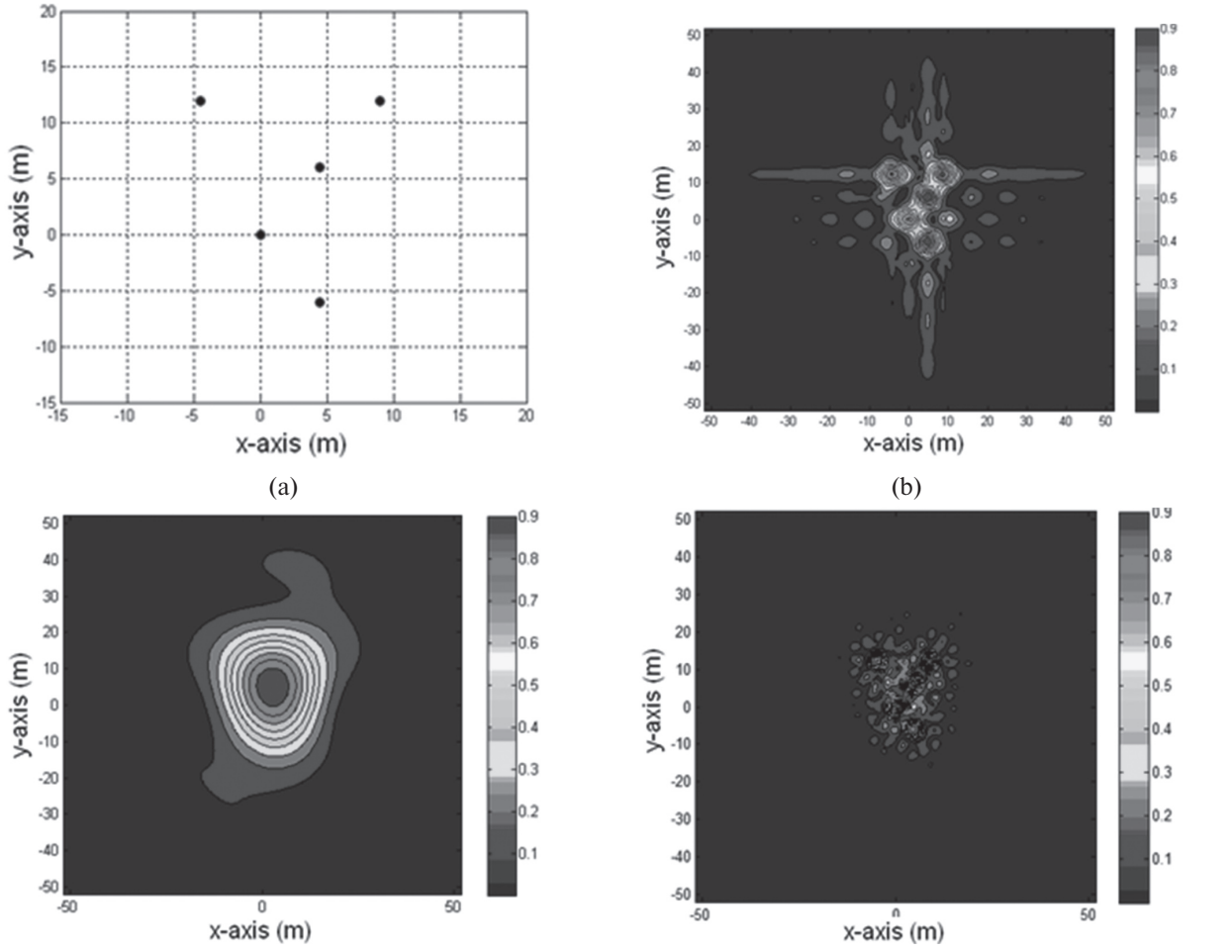

Fig. 9. Multiple target scene imaging protocols: (a) multiple target scene specification; (b) scene image in the *x-y* plane formed with the X-configured imaging array via implementing the technique (2); (c) the same scene image formed with the O-configured imaging array system; (d) the same scene image formed with the Y-configured (GeoSTAR) imaging array system. In all reported simulations, the images have been reconstructed from the data contaminated with additive zero-mean Gaussian noise with the same signal-to-noise ratio, SNR = 20 dB

regularized MSF procedure (2) (DED-MSF) can still operate within some admissible performance degradation level. In Fig. 12, the related simulation results are shown for the 4-NNI method (6).

IV. OPTIMIZATION OF GEOSTAR ARRAY CONFIGURATION

At the HW design level, three configuration "degrees of freedom" that we denote as $\{\gamma, d_A, D_s\}$ influence the overall PSF performances. In particular, parameter γ specifies the adopted array geometry (X, O or Y); d_A is the inter-element spacing, and D_s represents the effective aperture width of a single sensor. Unfortunately, no unique criterion exists for balanced optimization of $\{\gamma, d_A, D_s\}$ aimed at minimization of the resolution cell width over the balanced suppression of the PSF side lobes [6], [11].

That is why, in this study, we perform the solution to the HW-level optimization problem employing a new quality metric that we construct following the general DED framework [4], [5] for minimization of the energy of the main beam (E_M) of the PSF balanced over the normalized energy of the PSF side lobes (E_S). That is, we construct the PSF shape metrics μ_1 (that characterizes the quality of spatial resolution) to be proportional to the energy of the main beam E_M and

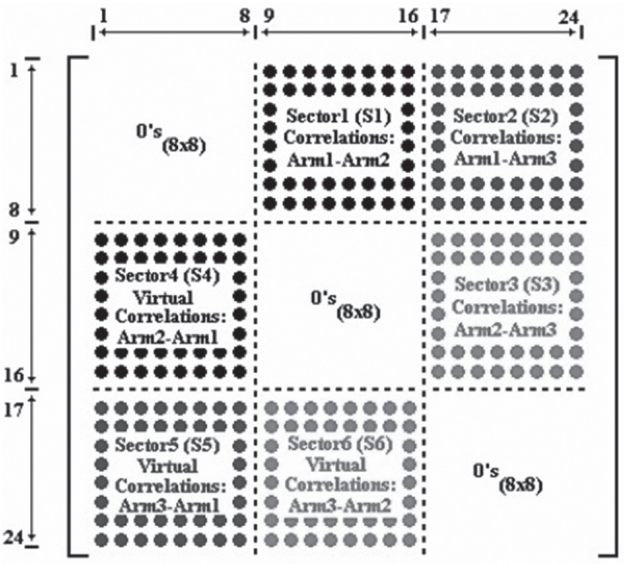

Fig. 10. Illustrating the structure of the DED-sparse GeoSTAR-configured MAR system data correlation matrix $\mathbf{Y}_r$ (collected data signal visibilities)

inversely proportional to the energy of the PSF side lobes energy norm E_S scaled by the factor C_M, i.e.,

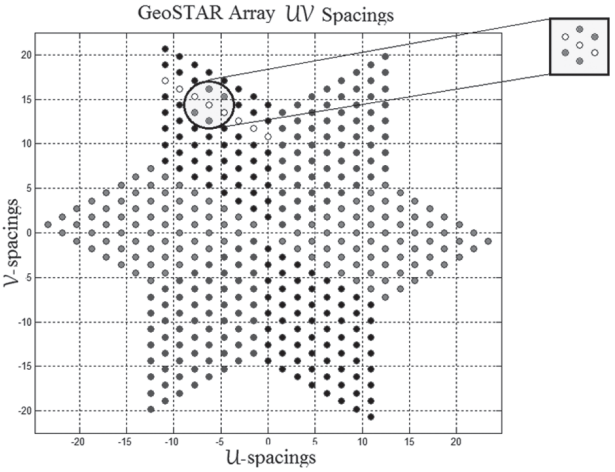

Fig. 11. Graphical description of the 4-NNI algorithm for reconstruction of matrix $\mathbf{Y}_r$ (in the visibility function domain)

$$\mu_1(\gamma, d_A, D_s) = \frac{E_M(\gamma, d_A, D_s)}{E_S(\gamma, d_A, D_s) C_M(\gamma, d_A, D_s)} \quad (7)$$

where the scaling factor

$$C_M(\gamma, d_A, D_s) = \frac{mes_{(0.5)} MB(\gamma, d_A, D_s)}{mes._{(0.1)} SL(\gamma, d_A, D_s)} \quad (8)$$

is calculated by measuring the main beam area $mes_{(0.5)}$ (MB) at 0.5 threshold from its maximum level normalized by the corresponding side lobes area $mes_{(0.1)}$ (SL) measured at 0.1 threshold from the PSF maximum level. We address this metric (7) as an indicator of the efficiency of the employed array configuration subject to three controllable geometrical degrees of freedom (interelement spacing, antenna array geometry and the effective aperture width of a single sensor). In Fig. 13, the performance metric (7) is presented for 10 possible tested inter-element spacings, in particular, $d_{A(1)} = 0.5\lambda_o$, $d_{A(2)} = 0.8\lambda_o$, $d_{A(3)} = 1\lambda_o$, $d_{A(4)} = 1.5\lambda_o$, $d_{A(5)} = 1.8\lambda_o$, $d_{A(6)} = 2\lambda_o$, $d_{A(7)} = 2.5\lambda_o$, $d_{A(8)} = 3\lambda_o$, $d_{A(9)} = 3.5\lambda_o$, and $d_{A(10)} = 4\lambda_o$, with a field of view of 60°. This metric can be also referred to as a normalized probability of target detection [11]. From the analysis of these data of Fig. 13, it follows that the best imaging and detection performances evaluated via metric (7) is achieved with $d_{A(6)} = 2\lambda_o$ as it was previously previsioned in [11].

To quantify the imaging performance in the harsh operational scenarios, we also employed the conventional signal-to-noise improvement (SNI) metric

$$\mu_2 = \frac{\sum_{(x_i, y_j)} |picId - picN|^2}{\sum_{(x_i, y_j)} |picId - picOb|^2} \quad i, j = 1, \ldots, N \quad (9)$$

where N represents the number of pixels in the image scene (at a particular range gate), $picId$ is the hypothetical ideal image, $picN$ is the MSF image formed

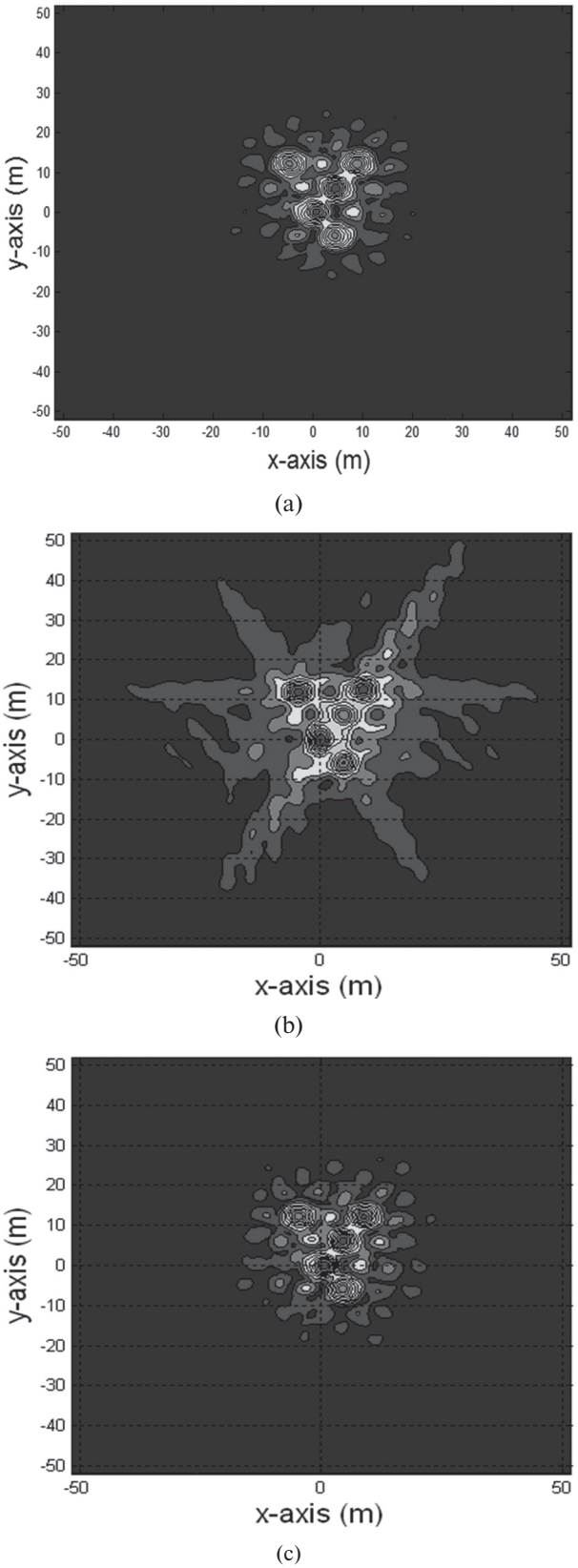

Fig. 12. Multiple target scene imaging protocols for 2λ inter-element spacing: (a) TAGs scene image in the x-y plane formed with the Y-configured imaging array via implementing the MSF technique (2) for 30m range gate (scenario without operational uncertainties); (b) scene image formed for the same range gate with 5 disabled sensors (without employing any correcting algorithm); (c) the same scene image with the same 5 disabled sensors formed via aggregating the MSF technique (2) with the 4-NNI method (6). All scene images have been reconstructed from the data contaminated with additive zero-mean Gaussian noise with the same signal-to-noise ratio, SNR = 20 dB

in a scenario without operational uncertainties and *picOb* is the corresponding DED-MSF image formed in a harsh (uncertain) scenario. The difference between the desired image and the actually formed distorted image is calculated via (9). In Fig. 14 the SNI values (9) are presented in a graphical format.

As it was mentioned before, one of the goals of the undertaken analysis is to determine the maximal number of disabled sensors with which the MAR that employs the DED-MSF method (2) can still operate within some performance degradation tolerance level. It is reasonably to specify such the level via the admissible SNI losses, e.g., –3 dB SNI losses.

Based on the analysis of the performances reported in Fig. 14, one may conclude that at the admissible –3 dB SNI loss threshold level, the DED-MSF (2) can still operate with up to 7 disabled sensors when aggregated with the DED regularized 4-NNI technique (6).

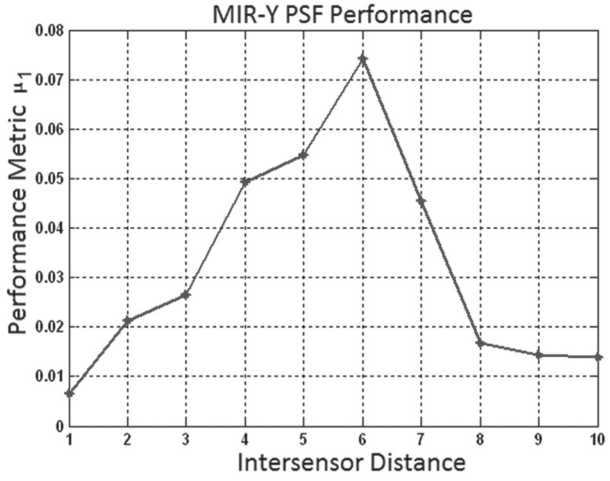

Fig 13. μ_1 metric for the MAR-MSF technique (2) for Y-configured MAR

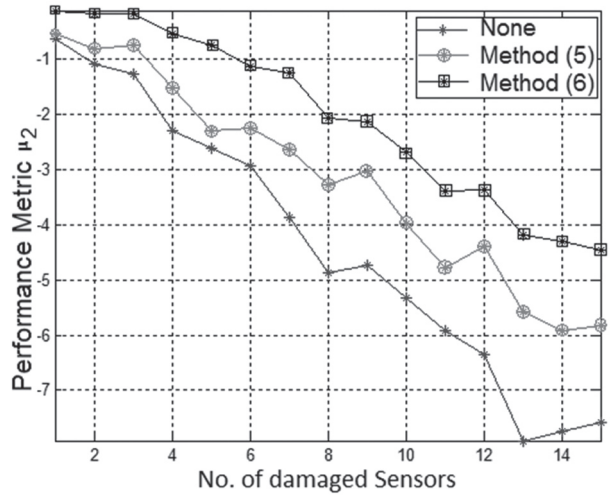

Fig 14. μ_2 metric for the MAR-MSF technique (2) for Y-configured MAR. The μ_2 metric characterizes the SNI loses dependent of the number of disabled sensors

DISCUSSIONS AND CONCLUDING REMARKS

We have addressed the new robust DED approach for enhanced imaging of multiple target scenes in harsh operational environments directly adapted to MAR imaging systems with different array configurations. We have also presented the detailed analysis of operational performances for uncertain operational scenarios, in particular, with antenna array sensor displacement due to damage or manufacturing errors and/or some possibly disabled sensors. The reported performance analysis establishes the tolerance to such harsh operational uncertainties admissible with the proposed robust DED-MSF imaging procedure.

The presented high-resolution target localization protocols are indicative of the superior operational efficiency of the Y-configured multimode imaging MAR system with the adopted GeoSTAR array geometry. The reported PSFs provide explicit information on the spatial resolution achievable with such MAR system that employs the proposed DED-robustified MAR-MSF image formation technique. We demonstrated via the analysis of behavior of μ_1 quality metric that the inter-element sensor spacing $d_{A(6)} = 2\lambda_o$ yields the best imaging performances for the 60° adopted field of view; the larger inter element spacings ($d_A > 2\lambda$) result in undesirably high artifacts (inadmissibly high grating sidelobes level) that is strongly undesirable for the target localization problems. For the purpose of precise multiple target localization, we established an admissible SNI loss threshold of –3 dB and found that the robustified DEDR-MSF technique admits operating for up to 7 disabled sensors. In future studies, we intend to focus on the HW-SW co-design aimed at the resolution enhancement of the DED-MSF imagery and approaching the super-resolution imaging performances with MAR systems.

REFERENCES.

[1] A.B. Tanner *et al*, "Initial Results of the Geosynchronous Synthetic Thinned Aperture Radiometer (GeoSTAR)", *IEEE Inern. Symposium on Geoscience and Remote Sensing, IEEE IGARSS 2006*, ISBN 0-7803-9510-7/06, pp. 3951-3954, 2006.

[2] Y. Shkvarko, "Estimation of wavefield power distribution in the remotely sensed environment: Bayesian maximum entropy approach", *IEEE Trans. Signal Proc.*, vol. 50, No. 9, pp. 2333-2346, 2002.

[3] Y. Shkvarko, "Unifying regularization and Bayesian estimation methods for enhanced imaging with remotely sensed data—Part I: Theory", *IEEE Trans. Geoscience and Remote Sensing*, vol. 42, No. 5, pp. 923-931, (2004).

[4] Y. Shkvarko, "From matched spatial filtering towards the fused statistical descriptive regularization method for enhanced radar imaging", *EURASIP J. on Applied Signal Processing*, vol. 2006, Article ID 39657, pp. 1-9. (2006).

[5] Y. Shkvarko, "Unifying experiment design and convex regularization techniques for enhanced imaging with uncertain remote sensing data—Part I: Theory", *IEEE Trans. Geoscience and Remote Sensing*, vol. 48, No. 1, pp. 82-111, 2010.

[6] Y. Shkvarko and V. Espadas, "Experiment Design Framework For Super-High Resolution Imaging With The GeoSTAR Configured Sensor Array Data", *The Seventh International Kharkov Symposium on Physics and engineering of Microwaves, Milimiter and Submilimiter Waves MSMW'10, ,* ISBN 978-1-4244-7898-9/10, 2010.

[7] *Principles and Applications of Imaging Radar*, *Manual of Remote Sensing*, 3d ed., F.M. Henderson and A. V. Lewis, Eds., vol. 3, NY: Willey, 1998.

[8] H.H. Barrett and K.J. Myers, *Foundations of Image Science*, NY: Willey, 2004.

[9] J.C. Curlander and R. McDonough, *Synthetic Aperture Radar––System and Signal Processing.* NY: Wiley, 1991..

[10] D.R. Wehner, *High-Resolution Radar*, 2nd ed., Boston, MA: Artech House, 1994.

[11] Y. Shkvarko, V. Espadas, and D. Castro, "Descriptive Experiment Design Optimization of GeoSTAR Configured Multisensor Imaging Radar", *4th International Radio Electronics Forum* (4th IREF'2011), Kharkov, Ukraine, Vol. I, pp. 76-81, Oct. 2011

Manuscript received February, 14, 2013

V. E. Espadas (S'10) was born in Merida, Yucatan, Mexico, on May 17, 1985. He received his Bachelor of Science degree in Electronic Engineering from the Institute of Technology of Merida (ITM), Merida, Mexico, in 2008 and the M.Sc. degree in Electrical Engineering from the Centro de Investigaciyn y de Estudios Avanzados del Instituto Politйcnico Nacional (Superior Education and Research Center of the National Polytechnic Institute of Mexico, CINVESTAV-IPN), Guadalajara, Mexico, in 2011. He is currently working towards the Ph.D. degree at the Department of Electrical Engineering, Communications Division, at the CINVESTAV-IPN. His research interests are in applications of signal processing of remote sensing, radar imagery, statistical sensor array data processing and communications.

Yuriy V. Shkvarko (M'95–SM'04) received the Dip. Eng. (Hon.) degree in electrical engineering, the Ph.D. degree in radio engineering, and the Dr. Sci. degree in radio physics, radar, and navigation from the Kharkov Aviation Institute, Kharkov, Ukraine, in 1976, 1980, and 1990, respectively. From 1976 to 1991, he was with the Scientific Research Department of the Kharkov Aviation Institute (presently National Airspace University of Ukraine), as a Research Fellow, a Senior Fellow, and a Chair of the Research Laboratory in information technologies for radar and navigation. From 1991 to 1999, he was a Full Professor with the Department of System Analysis and Control, Ukrainian National Polytechnic Institute, Kharkov. From 1999 to 2001 he was an Invited Professor with the Guanajuato State University at Salamanca, Mexico. Since 2001, he has been with the "Centro de Investigaciyn y de Estudios Avanzados del Instituto Politйcnico Nacional" (Superior Education and Research Center of the National Polytechnic Institute of Mexico), Guadalajara, Mexico, as a Full Titular Professor. He holds 12 patents and has published two books and some 160 journal and conference papers. His research interests are in applications of signal processing to remote sensing, imaging radar, navigation, and communications, particularly in inverse problems, random fields estimation, adaptive spatial analysis, statistical sensor array and multimode remote sensing data processing, and system fusion.

УДК 621.396

Метод регуляризации на основе дескриптивного планирования экспериментов для формирования высокоразрешающих радиоизображений в мультимодальных РЛС с антенными решетками / В.Э. Эспадас, Ю.В. Шкварко // Прикладная радиоэлектроника. – 2013. Том 12. № 1. – С. 157-165.

Предложен новый метод регуляризации обратных задач формирования радиолокационных (РЛ) изображений с улучшенным разрешением на основе теории дескриптивного планирования экспериментов (ДПЭ) дистанционного зондирования. Для необходимой избыточности РЛ измерений используется многомодовая поляризация, позволяющая комплексировать РЛ изображения отдельных мод и обеспечить робастность обработки сигналов в различных операционных сценариях. Предложенный ДПЭ-подход осуществляет робастную модификацию метода Ван-Циттерта — Цернике для РЛС с антенными решетками. Метод реализуется в форме банка согласованных фильтров формирования РЛ изображений на различных модах. Форма результирующей вещественной функции неопределенности оптимизируется на основе метода ДПЭ-регуляризации, который реализует оптимальный баланс между повышением разрешения и фильтрации помех, адаптированный к сценариям визуализации множественных целей в условиях статистической априорной неопределенности. Численное моделирование подтверждает эффективность предложенного метода формирования высокоразрешающих РЛ изображений множественных целей в статистически неопределенных операционных сценариях.

Ключевые слова: антенная решетка, дескриптивное планирование экспериментов, многомодовая РЛС формирования изображений, регуляризация.

Ил. 14. Библиогр.: 11 назв.

УДК 621.396

Метод регулярізації на основі дескриптивного планування експериментів для формування високорозрізняючих радіозображень в мультимодальних РЛС з антенними решітками / В.Е. Еспадас, Ю.В. Шкварко // Прикладна радіоелектроніка. – 2013. Том 12. № 1. – С. 157-165.

Запропоновано новий метод регуляризації обернених задач формування радіолокаційних (РЛ) зображень з покращеним розрізненням на основі теорії дескриптивного планування експериментів (ДПЕ) дистанційного зондування. Для забезпечення необхідної надмірності РЛ вимірювань використовується багатомодова поляризація, що дозволяє скомплексувати РЛ зображення окремих мод і забезпечити робасність обробки сигналів у різних операційних сценаріях. Запропонований ДПЕ-підхід здійснює робастну модифікацію методу Ван-Циттерта — Церніке для РЛС з антенними решітками. Метод реалізується у формі банку узгоджених фільтрів формування РЛ зображень на різних модах. Форма результуючої дійсної функції невизначеності оптимізується на основі методу ДПЕ-регуляризації, який реалізує оптимальний баланс між підвищенням розрізнення та фільтрації перешкод, адаптований до сценаріїв візуалізації множини цілей в умовах статистичної апріорної невизначеності. Кількісне моделювання підтверджує ефективність запропонованого методу формування високорозрізняючих РЛ зображень множини цілей у статистично невизначених операційних сценаріях.

Ключові слова: антенна решітка, дескриптивне планування експериментів, багатомодова РЛС формування зображень, регуляризація.

Іл. 14. Бібліогр.: 11 найм.